Remote Sensing of Environment 143 (2014) 216–227

Contents lists available at ScienceDirect

Remote Sensing of Environment

journal homepage: www.elsevier.com/locate/rse

Changes in aerosol optical properties due to dust storms in the Middle East and Southwest Asia

Khan Alam [a,*], Thomas Trautmann [b], Thomas Blaschke [c], Fazli Subhan [d]

[a] Institute of Physics and Electronics, University of Peshawar, Khyber Pakhtunkhwa, Pakistan
[b] German Aerospace Centre, Remote Sensing Technology Institute, Oberpfaffenhofen, 82234 Wessling, Germany
[c] Department of Geoinformatics Z_GIS, University of Salzburg, Hellbrunner Strasse 34, 5020 Salzburg, Austria
[d] Government Post graduate College, Swabi, KPK, Pakistan

ARTICLE INFO

Article history:
Received 23 September 2013
Received in revised form 23 November 2013
Accepted 29 December 2013
Available online xxxx

Keywords:
Dust storms
AOD
Size distribution
SSA
Radiative forcing

ABSTRACT

Super dust storms occurred over the Middle East and southwest Asia on March 2012. These storms reduced the air quality over the Gulf Region, Iraq, Iran, and Pakistan. Airports were shut down due to poor visibility, schools were closed, and hundreds of people were hospitalized with respiratory problems. In order to better understand the effects of such dust storms we have analyzed aerosol optical and radiative properties during this event using data from the Moderate Resolution Imaging Spectroradiometer and the Aerosol Robotic Network. Maximum aerosol optical depth (AOD) values occurred on the18th of March in Kuwait, Bahrain, Qatar, and Saudi Arabia, where values of 4.9, 4.4, 4.3, and 4.9 were recorded, respectively. In Oman, the Arabian Sea, and Iran, maximum AOD values occurred on the 19th of March, reaching 4.5, 5, and 5, respectively. The dust storm then spread across Pakistan, passing through Multan, Faisalabad, and Lahore where maximum AOD values of 2.1, 2.6, and 2.7, respectively, were attained on the 20th of March. The maximum aerosol volume size distributions (VSDs) in Lahore occurred on dusty days and minimum VSDs on non-dusty days. The VSD, single scattering albedo, refractive index, and asymmetry parameter values on dusty days suggested that dust aerosols were predominant over anthropogenic aerosols in these urban environments. The shortwave aerosol radiative forcing (ARF) values (on both dusty and non-dusty days) ranged between -50 W m^{-2} and -194 W m^{-2} (average: -114 ± 40 W m^{-2}) at the earth's surface, and between -31 W m^{-2} and -105 W m^{-2} (average: -58 ± 25 W m^{-2}) at the top of the atmosphere (TOA). The longwave aerosol ARF values ranged between $+6$ W m^{-2} and $+20$ W m^{-2} (average: $+12 \pm 4$ W m^{-2}) at the earth's surface, and between $+7$ W m^{-2} and $+30$ W m^{-2} (average: $+16 \pm 7$ W m^{-2}) at the TOA. Longwave radiations therefore produced significant warming, both at the TOA and at the earth's surface.

1. Introduction

Dust storms cause significant perturbations in the radiation-energy balance of the earth's atmospheric system, in atmospheric heating and stability (Alpert, Kishcha, Shtivelman, Krichak, & Joseph, 2004), in chemical and biological ecosystems (Singh, Prasad, Kayetha, & Kafatos, 2008), and in ambient air quality and human health (Nastos, Kampanis, Giaouzaki, & Matzarakis, 2011). Different natural mineral dust particles may either absorb or scatter radiation (ultra violet, visible, and infrared), resulting in either "positive forcing", i.e. heating, or "negative forcing", i.e. cooling (Alpert et al., 1998; Liao & Seinfeld, 1998; Miller, Perlwitz, & Tegen, 2004; Sinha & Harries, 1997; Sokolin & Toon, 1996; Tegen, Lacis, & Fung, 1996). Mineral dust aerosols reflect shortwave (SW) radiation within the atmospheric window channel back into space resulting in cooling of the Earth's system, but longwave (LW) radiation is absorbed resulting in a warming effect (Xia and Zong, 2009). Variations in the properties, transport, and dynamics of different mineral dust aerosols have been investigated by Almeida (1987), Prospero and Carlson (1972), and Tegen and Fung (1994). Dust storms can have considerable impacts on the hydrological cycle, on climate variability, and on ambient air quality (Golitsyn & Gillette, 1993; Kaufman, Tanre', & Boucher, 2002; Miller, Tegen, & Perlwitz, 2004; Parungo et al., 1995; Prospero, Ginoux, Torres, Nicholson, & Gill, 2002; Ramanathan, Crutzen, Kiehl, & Rosenfeld, 2001; Tegen et al., 1996).

Dust particles can alter the surface radiation budget leading to changes in the temperature of the earth's surface and consequently influencing the exchange processes between the earth's surface and atmosphere, as well as atmospheric dynamics. Accurate estimation of the radiative impact of mineral dust storms is therefore important, particularly because of their broad spatial distributions and large optical depths (Mishra and Tripathi, 2008). Changes in the aerosol radiative forcing (ARF) of the troposphere due to dust storm activity over the western Sahara Desert and eastern tropical North Atlantic Ocean have previously been investigated by Alpert et al. (1998). The vertical distribution of dust aerosols has a large influence on RF, and on the climate (Forster et al., 2007;Huang et al., 2009; Zhu et al., 2007). Liao and Seinfeld (1998) reported that clear-sky long-wave RF and cloudy sky top-of-

* Corresponding author. Tel.: +92 300 2514177.
E-mail address: khanalam@upesh.edu.pk (K. Alam).

0034-4257/$ – see front matter © 2014 Elsevier Inc. All rights reserved.
http://dx.doi.org/10.1016/j.rse.2013.12.021

atmosphere (TOA) SW RF are very sensitive to the dust layer. Mineral dust has also been found to be the main factor affecting aerosol optical depth (AOD) in various arid regions of the world (Houghton et al., 2001; Tegen et al., 1997).

Dust storms originating from arid and desert areas in Africa (e.g., the Sahara Desert), the Middle East, Saudi Arabia, and India (e.g., the Thar Desert) often travel to the coastal areas of Pakistan and contribute to the total aerosol loading over various regions of Pakistan. Variations in the optical properties of dust aerosols over the Indo-Gangetic plains have been reported by Prasad et al. (Prasad and Singh, 2007; Prasad et al., 2007). Some general optical properties of dust aerosol over Lahore and Karachi have previously been analyzed by Alam, Trautmann, and Blaschke (2012) using AERONET data, and the frequency of dust storms over southwest Asia has been discussed by Husar et al. (2001) and Middleton (1986).

Dust storms result in changes to aerosol loading in the troposphere over southwest Asia during the pre-monsoon season and influence the rainfall distribution because dust aerosols alter the earth's radiative balance, either directly by extinguishing solar and Earth radiation, or indirectly by acting as, or enhancing, cloud condensation nuclei (CCN), thereby affecting the cloud albedo, cloud lifetime, precipitation rate, and hydrological cycle (Charlson & Heintzenberg, 1995; Hansen, Sato, & Ruedy, 1997). Changes in radiative forcing have an effect on the monsoonal circulation and such changes induced by dust storms can have a major influence on the strength of the monsoon (Miller & Tegen, 1998; Ramanathan et al., 2001). Ground-based observations and satellite data are very important for monitoring dust events and estimating ARF.

In this study we have used Moderate Resolution Imaging Spectroradiometer (MODIS) data to analyze aerosol properties over the Middle East and southwest Asia during dust storms that several meteorologists have characterized as super dust storm (NASA Earth Observatory Natural Hazards, 2012). We also investigated aerosol optical and radiative properties over Lahore (Pakistan) during dusty and non-dusty days on March 2012 using both Aerosol Robotic Network (AERONET) and MODIS data. The pathways and possible source regions for the dust storm events were also investigated by back-trajectory analysis using a Hybrid Single Particle Lagrangian Integrated Trajectory (HYSPLIT) model. In addition to aerosol characteristics, ARF values at the earth's surface and at the TOA were calculated for different episodes of the dust storm using the Santa Barbara DISORT Atmospheric Radiative Transfer (SBDART) model (Ricchiazzi, Yang, Gautier, & Sowle, 1998).

2. Data

Spatio-temporal variations in AOD during the strong dust storm event over the Middle East and southwest Asia were analyzed using MODIS data. It was also considered to be important to analyze the aerosol characteristics, including optical and radiative properties, during the dust storm, for which AERONET data would have been the best option. Unfortunately however, AERONET data were not available over the dust storm period for the sites in Bahrain, Saudi Arabia, and Kuwait; we therefore used data from the Lahore AERONET site.

2.1. Aerosol Robotic Network (AERONET)

The CIMEL sky radiometer is the standard AERONET instrument for measuring direct sun and diffuse sky radiances within the 340–1020 nm and 440–1020 nm spectral ranges, respectively (Holben et al., 1998). An inversion algorithm was used to retrieve aerosol volume size distributions for radii ranging from 0.05 to 15 μm, while spectrally dependent complex refractive indexes (RIs), single scattering albedos (SSAs) and asymmetry (ASY) parameters were obtained from spectral sun and sky radiance data. The detailed aerosol properties retrieved were used for calculating broad brand fluxes within the spectral range from 0.2 to 4.0 μm. The AERONET data are available at three levels – level 1.0 (unscreened), level 1.5 (cloud screened; Smirnov et al., 2000), or level 2.0 (quality assured; Holben et al., 1998) – and can be downloaded from the AERONET website (http://aeronet.gsfc.nasa.gov/). For this study we used AERONET level 2.0 data from both direct sun (AOD) and inversion products (SSA, ASY, RI) for the month of March, 2012. The uncertainty in AOD retrieval under cloud-free conditions was $<\pm 0.01$ for wavelengths >440 nm, and $<\pm 0.02$ for shorter wavelengths, which is less than the $\pm 5\%$ uncertainty for the retrieval of sky radiance measurements (Dubovik et al., 2000). The retrieval accuracy has been explained in detail by Dubovik et al. (2002).

2.2. Moderate Resolution Imaging Spectroradiometer (MODIS)

MODIS instruments are installed on the Terra and Aqua satellites which were launched in December 1999 and May 2002, respectively. They offer high radiometric sensitivity (12 bit) over 36 spectral bands with wavelengths ranging from 0.41 μm to 14.4 μm. The spatial resolution of the MODIS instrument varies with the spectral band, ranging from 250 m to 1.0 km at nadir. The MODIS instruments offer an unprecedented opportunity to examine terrestrial, atmospheric, and oceanic phenomena around the world. MODIS instruments measure the AOD with an estimated error of $\pm(0.05 + 0.15\tau)$ over land (Chu et al., 2002) and 0.03 ± 0.05 over the ocean (Remer et al., 2005). The operational MODIS aerosol retrieval algorithm has recently been improved in order to correct systematic biases in the MODIS algorithm used previously (Levy et al., 2007; Remer et al., 2005). The MOD04 AOD daily data products from Terra and Aqua Deep Blue AOD with a spatial resolution of 10×10 km from 1st March to 31st March, 2012 are utilized in this study. We have chosen this Deep Blue AOD product for the desert regions (Saudi Arabia, Persian Gulf, southeast Iran, southwest Pakistan) rather than the standard AOD product. In addition, the MODIS surface albedo product was also used. More detailed information on algorithms for the retrieval of aerosol data is available at http://modis-atmos.gsfc.nasa.gov.

2.3. Cloud-Aerosol Lidar and Infrared Pathfinder Satellite Observation (CALIPSO)

CALIPSO was launched on 28 April 2006 to study radiative effects of aerosols and clouds on climate. CALIPSO carries the Cloud-Aerosol Lidar with Orthogonal Polarization (CALIOP), a two wavelength polarization Lidar (532 and 1064 nm). It provides information on the vertical distribution of aerosols and clouds, cloud particle phases, and classification of aerosol size (Winker, Hunt, & McGill, 2007). Detailed discussion on CALIPSO and its instruments is provided by Hunt et al. (2009) and Winker, Pelon, and McCormick (2003).

3. Results and discussion

3.1. Formation of dust events and meteorological situation

Iraq, Saudi Arabia, and the Persian Gulf form a hot-spot region that has reported the highest occurrence of dust storms (Kutiel & Furman, 2003). Dust storms in Saudi Arabia, the Persian Gulf, Iraq, and Iran, on the Arabian Peninsula, and in southwestern Pakistan are more frequent in spring and summer than in autumn and winter. Two separate dust storms occurred over the Middle East and southwest Asia in March, 2012.

Due to a high pressure zone that formed over eastern Syria on March 17th, 2012 and a low pressure zone over northern Iraq, winds accelerated rapidly towards Iraq resulting in the development of a super dust storm that quickly spread across Iraq. High temperatures increased the likelihood of a dust storm by rendering unstable the atmospheric layers close to the ground surface. Airborne dust particles were blown towards the southeast and into Saudi Arabia, and the resulting dust

storm spread over thousands of kilometers from Iraq to the Red Sea via Kuwait, Bahrain, Qatar, and Saudi Arabia (Fig. 1), and from the Red Sea to Afghanistan and Pakistan via Saudi Arabia, Oman, Iran and the Arabian Sea (Fig. 1). On March 18th dusty conditions reached the United Arab Emirates (UAE), but with a reduced intensity as the high pressure caused most of the dusty air to move clockwise into central Saudi Arabia and the Yemen. On March 19th the low and high pressures traveled eastward remaining in close proximity to each other, thus establishing steep pressure gradients over southeast Iran and southwest Pakistan that resulted in an unusually large second dust storm in the region. The dust storm then migrated southward towards Oman and the north-eastern coastlines of the UAE. On March 20th the dust storm spread eastwards towards Pakistan, reaching the cities of Multan, Faisalabad, and Lahore. On March 2012 dust storm reduced the air quality over the Gulf Region, Iraq, Iran, and Pakistan (Multan, Faisalabad, and Lahore). It disrupted air traffic in Fujairah (where visibility was down to less than 500 m and the airport was shut down) and Yemen, closed schools, and resulted in hundreds of people being sent to hospital with respiratory problems (Kazmi & Vaidya, 2012).

The plumes of second dust from the storm were thick enough to obscure the land and water surfaces from space. The dust whipped up by the storm came from the fine sediments of sand seas and transient lakes along the borders between Iran, Pakistan, and Afghanistan.

3.2. AOD variations during the dust storm

Variations in AOD during the March 2012 dust storms were studied using MODIS and AERONET data at a wavelength of 550 nm for various locations in the Middle East and south-west Asia, including Kuwait (Wafra), Bahrain, Qatar (Doha), Saudi Arabia (Riyadh), Oman (Muscat), the Arabian Sea, Iran (Chabahar), and Pakistan (Lahore). The maximum AODs in Kuwait, Bahrain, Qatar, and Saudi Arabia were recorded on the 18th of March, reaching values of 4.9, 4.4, 4.3, and 4.9 respectively (see Fig. 2 a, b, c, & d). The maximum AODs in Oman, over the Arabian Sea, and in Iran were recorded on the 19th of March, with values reaching 4.6, 5, and 5, respectively (Fig. 2 e, f, & g). The dust storm then traveled into Pakistan and passed over Multan, Faisalabad, and Lahore, where the maximum AOD values were 2.1, 2.6, and 2.7, respectively, recorded on the 20th of March. The intense dust storm was observed over Lahore on the 20th and 21st of March. The AOD variability on those days, based on AERONET level-2 data, is shown in Fig. 3 (a & b). The figure reveals that AOD values were greater than 2.4 on the 20th of March. The AOD on the 20th of March ranged from 1.95 to 2.45 with an average of 2.17 ± 0.13, while on the 21st of March the AOD ranged from 1.26 to 1.48 with an average of 1.38 ± 0.07. The dust was observed over Lahore on the 20th, 21st, and 22nd of March, with dust plumes captured by the MODIS Terra satellite these dates (Fig. 4). The dust, which reached a maximum on the 20th and 21st of March, originated from Iraq, southeast Iran, and southwest Pakistan. The two dust storms developed in Iraq and southeast Iran and southwest Pakistan and then traveled to the Gulf Region and then back to Pakistan.

The relationship between MODIS and AERONET AODs was additionally analyzed in order to confirm that MODIS AOD retrievals are good enough for the condition of this study. This is particularly important since AERONET AOD values were only available for Lahore site. The daily $MODIS_{AOD}$ and daily average of $AERONET_{AOD}$ data values were used for the month of March, 2012 over Lahore. For validation, the daily mean AODs of 500 nm from AERONET were first interpolated to a common wavelength of 550 nm of MODIS using the power law

$$AOD_{550nm} = AOD_{500nm}\left(550 / 500\right)^{-\alpha}$$

where α is the (440–870 nm) Angstrom exponent (Alam, Trautmann, & Blaschke, 2011).

Fig. 3c shows the comparison of $MODIS_{AOD}$ and $AERONET_{AOD}$ in March, 2012. The $MODIS_{AOD}$ values were highly correlated with that of $AERONET_{AOD}$, with a correlation coefficient of 0.96. The comparison showed that $MODIS_{AOD}$ values are in good agreement with that of $AERONET_{AOD}$ values. The results suggested that the MODIS sensor provided an excellent AOD estimate over Lahore.

The source of the dust storms and the path that it followed before reaching Lahore have been analyzed by computing seven day back-trajectories using the Hybrid Single Particle Lagrangian Integrated Trajectory (HYSPLIT) model (Draxler & Rolph, 2003). The meteorological input for the trajectory model was the Global Data Assimilation (GDAS) dataset (reprocessed from the U.S. National Centres for

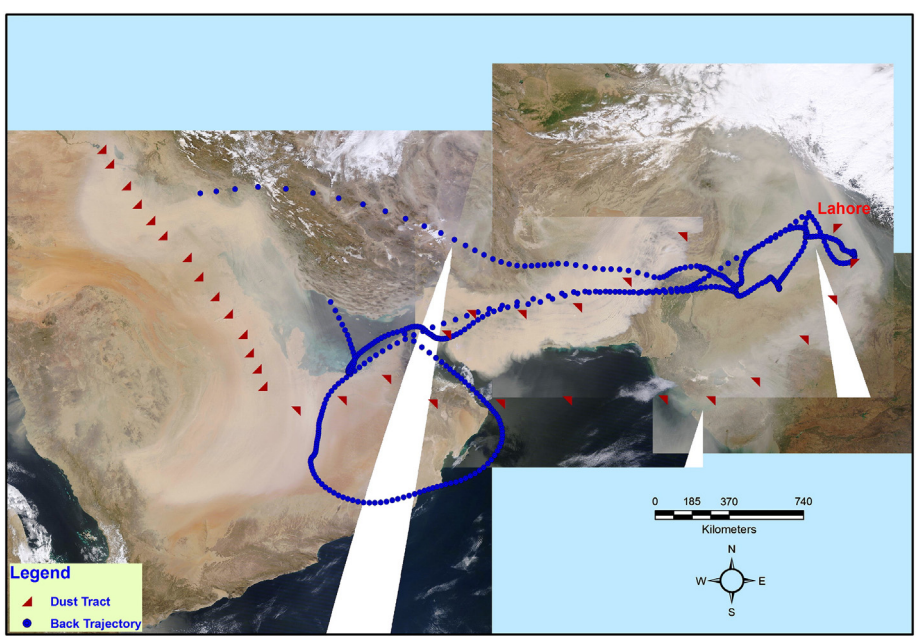

Fig. 1. The dust track along with back trajectory. The dust storms raging across southwest Asia and Middle East in March, 2012. The dust sweeping across Iraq, Saudi Arabia, Oman, Qatar, the United Arab Emirates, the Arabian Sea, Iran, and southwest Pakistan.

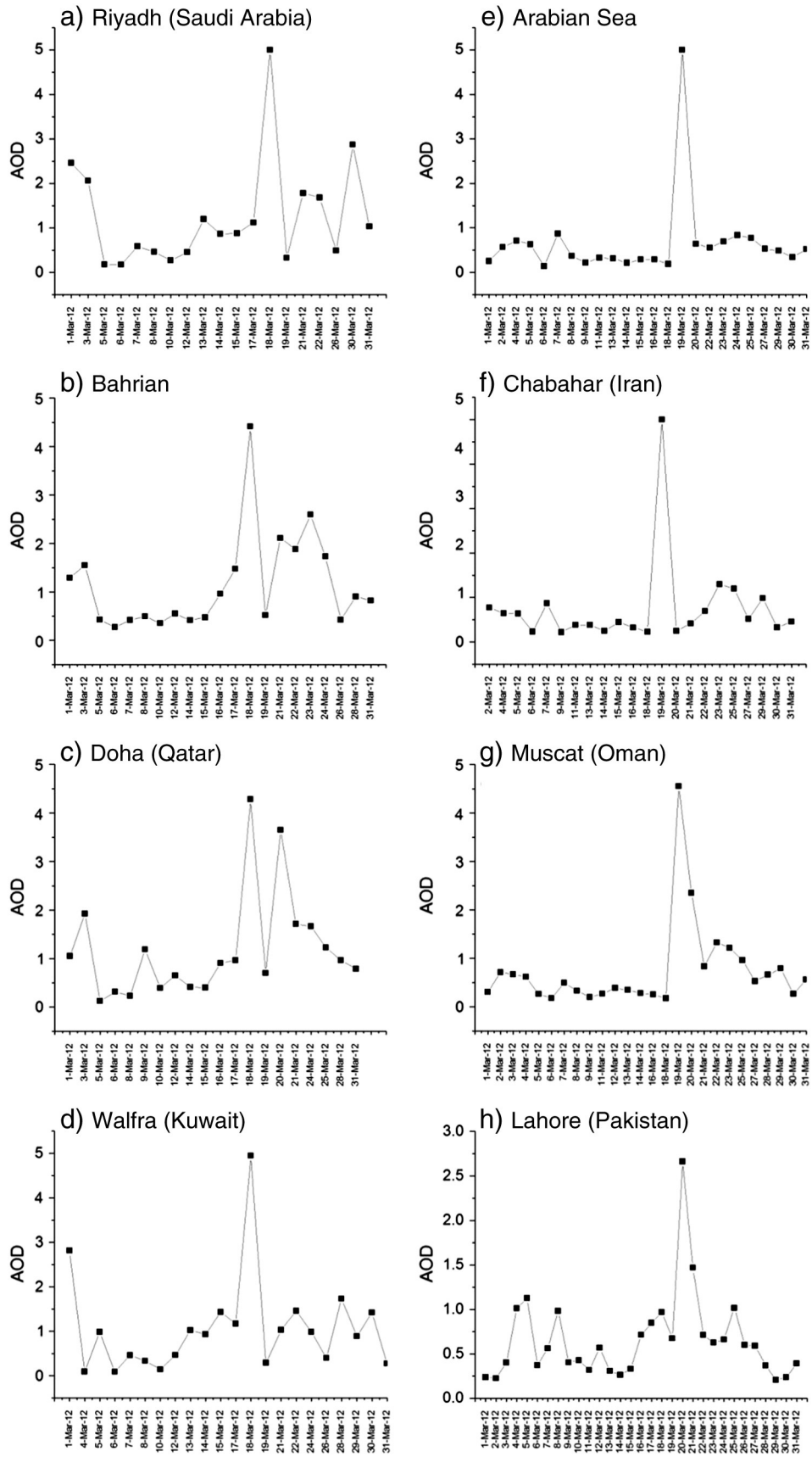

Fig. 2. Variability of MODIS AOD during dusty and non-dusty days over (a) Riyadh, (b) Bahrain, (c) Doha, (d) Wafra, (e) the Arabian Sea, (f) Chabahar, (g) Muscat, and (h) Lahore.

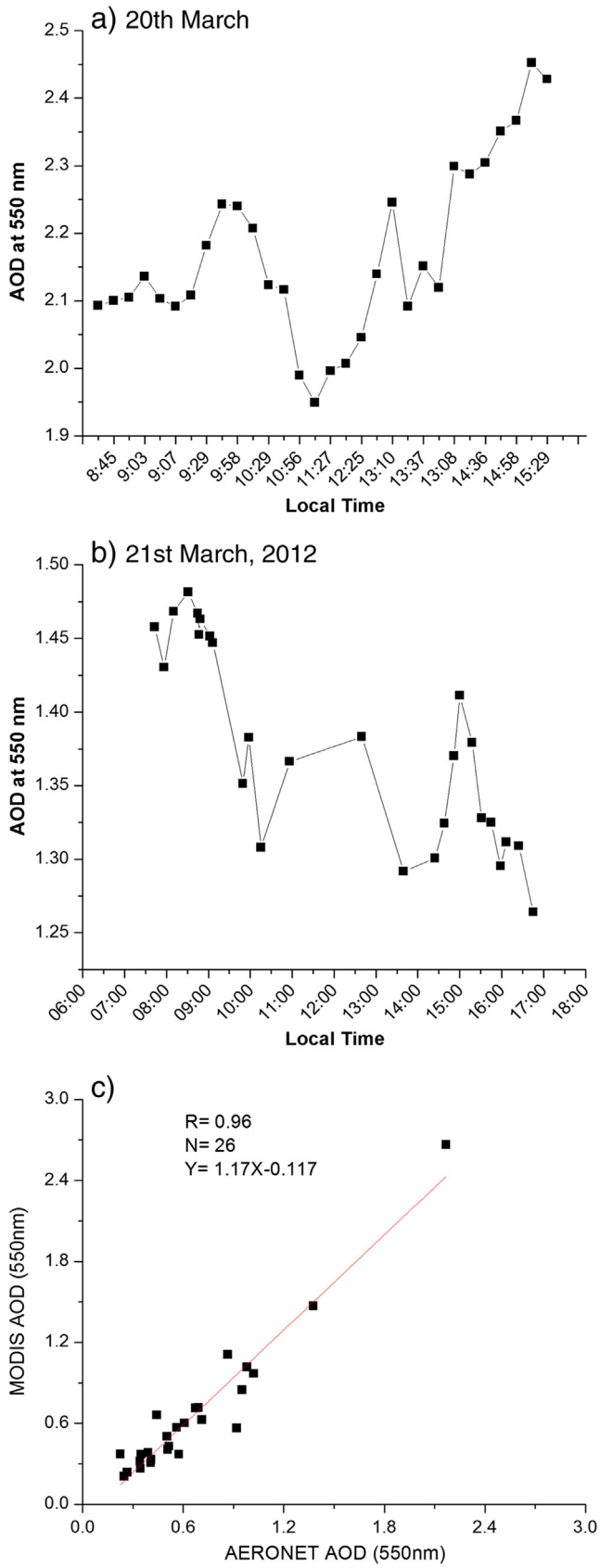

Fig. 3. Diurnal variations in AERONET AOD over Lahore on (a) the 20th March and (b) 21st of March. (c) Intercomparison between MODIS and AERONET AOD over Lahore.

Environmental Prediction by the Air Resources Laboratory). Since the AOD is a measure of columnar aerosol content, the back trajectories were computed within the studied region at three different altitudes above ground level (500 m, 1500 m, and 2500 m). The HYSPLIT back-trajectory analysis revealed that the air masses reached Lahore from Saudi Arabia, the UAE, Kuwait, and Iraq (see Fig. 5.). Local aerosol sources (e.g., locally derived dust due to industry, biomass burning, and vehicular emissions) can be seen to have contributed to an increase in aerosol concentrations over the cities in Pakistan (Alam, Blaschke, et al., 2011; Alam, Qureshi, et al., 2011; Alam, Trautmann, et al, 2011; Alam et al., 2012).

The aerosol subtype profile from Cloud-Aerosol Lidar and Infrared Pathfinder Satellite Observation (CALIPSO) measurements (https://www-calipso.larc.nasa.gov) on the 20th of March is shown in Fig. 5b. This figure reveals that a well-mixed dust layer occurred over the Lahore area in Pakistan (closest CALIPSO approach approximately 100–200 km). The aerosol types identified by CALIPSO in the vicinity of the study regions include both dust and polluted dust, but dust aerosols were dominant over the anthropogenic (polluted) aerosols. The CALIPSO aerosol profile indicated a layer of thick dust (carrying coarser particles) extending from the surface to an altitude of about 7 km (see Fig. 5b). The high aerosol concentrations over Lahore may therefore have been due to dust transported from afar, with lesser contributions from local sources.

3.3. Aerosol volume size distribution

The aerosol volume size distribution (VSD) is an important parameter due to the radiative impact that aerosol particles may have on climate. The AERONET aerosol VSD for March 2012 was determined from sun photometer measurements using 22 radius size bins ranging from 0.05 μm to 15 μm. The VSD has a two-mode structure that can be characterized by the sum of two lognormal distributions, as follows:

$$\frac{dV(r)}{dlnr} = \sum_{i=1}^{2} \frac{C_{v,i}}{\sqrt{2\pi}\sigma_i} \exp\left[\frac{\left(lnr - lnr_{v,i}\right)^2}{2\sigma_i^2}\right]$$

where σ_i is the standard deviation, $r_{v,i}$ is the volume median radius, and $C_{v,i}$ is the volume concentration for fine and coarse modes (Alam, Blaschke, et al., 2011; Xia et al., 2005; Zheng et al., 2008).

Fig. 6a illustrates the variation in the AERONET aerosol VSD during March 2012, showing a clear distinction between dusty and non-dusty days. There are two peaks, one between 0.05 and 0.25 μm and the other between 0.25 and 10 μm, representing two modes (fine and coarse) for the entire particle size distribution, i.e. fine and coarse modes for dusty (20th, 21st, and 22nd of March, 2012) and non-dusty days (15th, 17th, and 18th of March, 2012). The coarse mode aerosol particles (0.25–10 μm) show a significant increase in particle volume compared to non-dusty days, indicating the presence of mineral dust particles due to the dust storms. The different VSD peaks for dusty and non-dusty days are due to differences in other characteristics of the aerosol particles, as well as their radii. The peaks show a gradual increase in height as the AOD increases due to the dust storm. The maximum aerosol VSD peaks occurred at radii of 1.70 and 2.24 μm on the dusty-days, with the corresponding heights of the peaks being 1.69 and 1.57. These values are significantly higher than those reported by Prasad and Singh (2007) for dust storms that occurred between 2001 and 2005 over the Indo-Gangetic plains. The peaks of the maxima are sharp for the dusty days (20th and 21st of March) but relatively flat for the non-dusty days (15th, 17th, and 18th of March). Fig. 6b shows the diurnal variation in the AERONET aerosol VSD during dusty days (20th and 21st of March). The aerosol VSD values in the coarse mode are comparatively higher in the afternoon than in the morning. On the contrary, in the fine mode aerosol VSD values are a slightly higher in the morning than in the afternoon. The maximum aerosol VSD peak

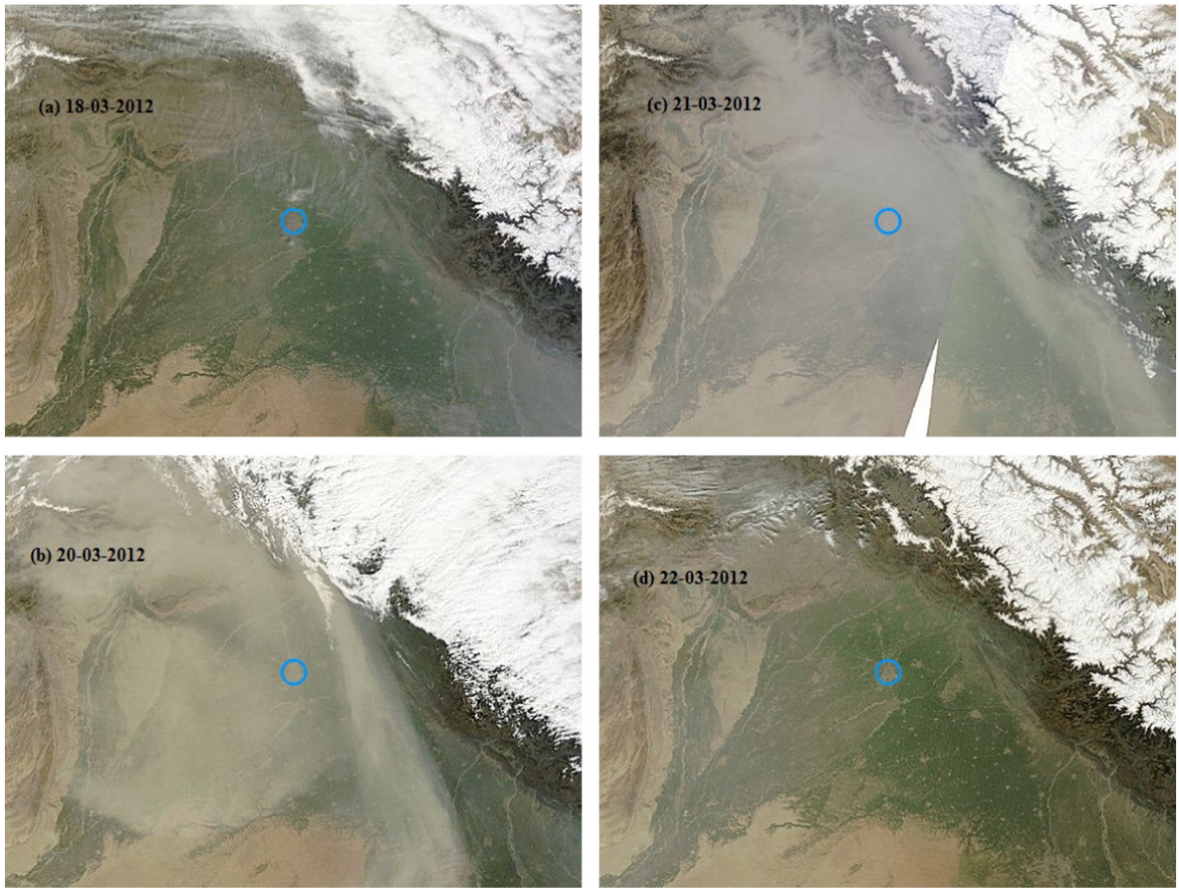

Fig. 4. MODIS derived spatial and temporal variations in dust over Lahore.

was 1.81 and this occurred at radius of 2.24 in the afternoon. The differences in diurnal variations of aerosol VSD during the dusty days are in the range from 0.10 to 0.24. The coarse mode aerosol VSD showed a 3 to 6-fold increase during the dust event compared to non-dusty days, whereas no significant change was observed in the fine mode aerosol VSD. A very similar variation in aerosol VSD during dust events has also been reported over the Indo-Gangetic Basin (Dey, Tripathi, Singh, & Holben, 2004).

3.4. Single scattering albedo and asymmetry parameter

The single scattering albedo (SSA) and the asymmetry (ASY) parameters are very important for determining the aerosol radiative forcing effects (Alam et al., 2012). The SSA is the ratio of the scattering efficiency to the total extinction efficiency of the dust particles and provides important information on the scattering and absorption properties of aerosols. This paper focuses on optical properties and solar heating effects during the dust storm over Lahore and column-averaged data from AERONET were therefore used to characterize the variability of these radiatively relevant parameters during the dust storm in March, 2012. The SSA is determined by the extinction optical thickness τ_{ext} (λ) and the scattering optical thickness τ_{scatt} (λ). The procedure involved in the retrieval of the SSA has been discussed by Dubovik et al. (2000). Fig. 7a shows the variability of the SSA during dusty and non-dusty days. There is a large increase in the SSA on dusty days compared to non-dusty days, for all wavelengths (440, 675, 870, and 1020 nm). The SSA varied from 0.87 to 0.95 on non-dusty days, and from 0.92 to 0.99 on dusty days. The maximum SSA value of 0.99 occurred at a wavelength of 1020 nm, which is an indication of the dust aerosol. The SSA increased with wavelength suggesting that the SSA is wavelength dependent; it increased with wavelength on both dusty and non-dusty days. This increase in SSA with wavelength shows that aerosol particles are predominantly scattering in behavior and larger in size, instead of absorbing particles (Dey et al., 2004; Shettle & Fenn, 1979). Fig. 7b illustrates the diurnal variations in SSA during dusty days (March 20th and 21st). The results revealed that SSA variation on the 20th of March is higher than on the 21st of March. The differences in diurnal variations in SSA on dusty days at a wavelength of 440 nm are in the range of 0.002–0.04. Likewise, the differences in diurnal variations in SSA at 1020 nm on dusty days are in the range of 0.0008–0.01. Dubovik et al. (2002) found the spectral difference in ΔSSA ($SSA_{1020\ nm} - SSA_{440\ nm}$) to be greater than 0.05 for mineral dust particles. Prasad et al. (2007) calculated ΔSSA during dusty days, which were 0.051, 0.060, 0.061, 0.070 and 0.073. Our results also match very well with the results made by Dubovik et al. (2002) and Prasad and Singh (2007). In our study the spectral difference ΔSSA was 0.073 and 0.074 for dusty days (March 20th and 21st, respectively). The maximum SSA values, which occurred on dusty days, were 0.99 and 0.98 on the 20th and 21st of March, respectively, at a wavelength of 1020 nm. The SSA reported during the dust storm that occurred over south Asia in 2010 was 0.925 (Dey et al., 2004; Sharma, Singh, & Kaskaoutis, 2012). The SSA of dust particles over eastern Asia (China) has been found to be around 0.90 at 500 nm. Low SSA values were recorded by Kim et al. (2004a, 2004b) during dust storms over Korea and Japan and the optical properties of these dust storms were shown to be similar to those of their dust source regions around Dunhuang in western China and Mandalgovi in Mongolia. The SSA values for dust storms over eastern Asia (China–Japan) have been observed to decrease with higher wavelengths. This was interpreted as being due to mixing with the large pool of anthropogenic aerosol pollution derived from absorbing soot and organic aerosols from fossil fuel

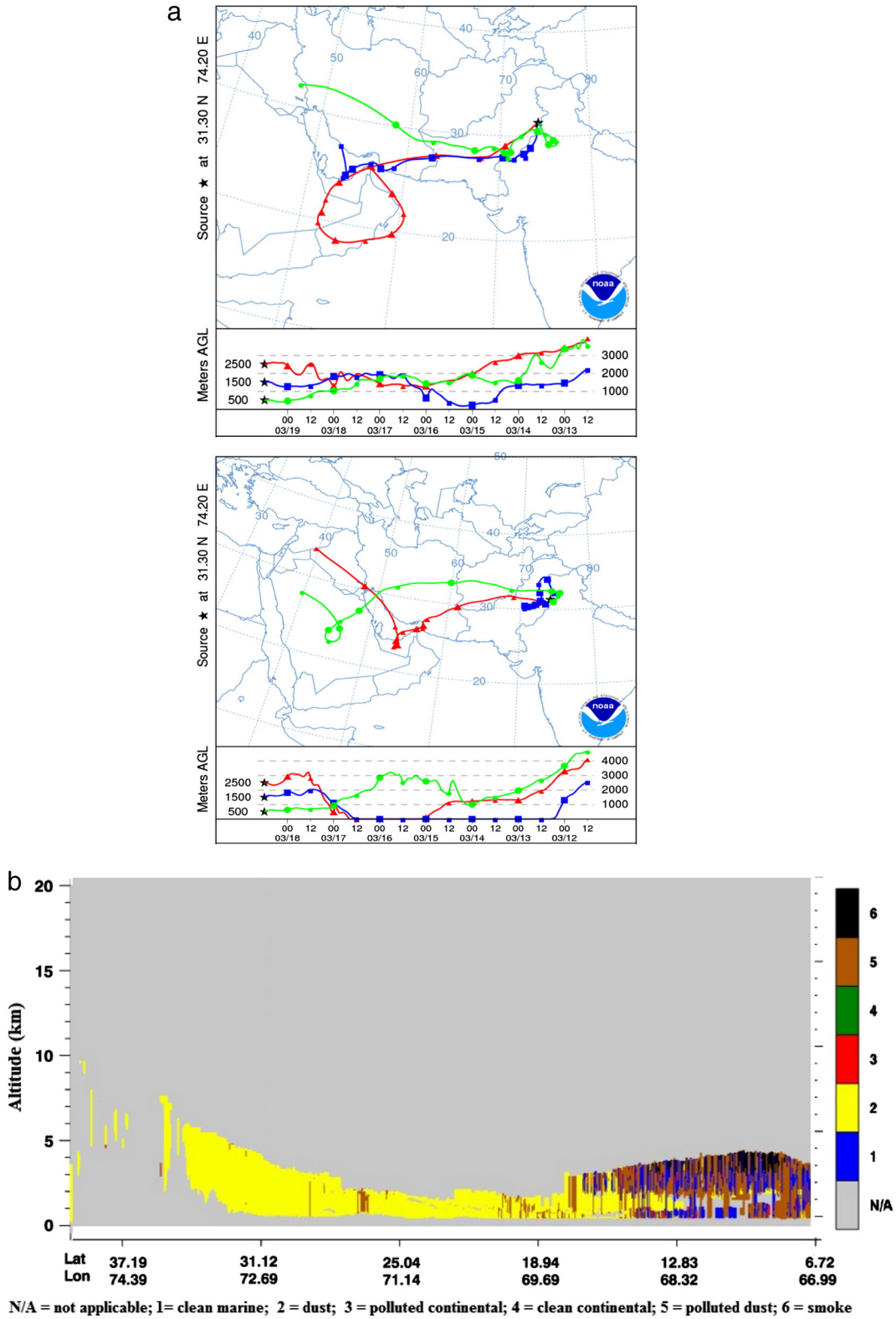

Fig. 5. (a) Seven-day back-trajectories ending at Lahore on the 18th and 19th of March, 2012. (b) CALIPSO retrieved aerosol classification (sub-type profile) over the studied region.

combustion (coal–petroleum), and from the burning of biomass (Chameides, Yu, Liu, et al., 1999).

The ASY is the cosine-weighted average of the scattering angle for the scattered radiation:

$$\mathrm{ASY}(\lambda) = \frac{1}{2}\int_0^{\pi} \cos(\theta) P(\lambda, \theta) \sin(\theta) d\theta$$

where θ is the angle between the incident and scattered radiation and $P(\lambda,\theta)$ is the phase function (angular distribution of scattered light).

The ASY is dependent on the size and composition of the particles and is a key property controlling the aerosol contribution to radiative forcing. The situation for which ASY = 1 corresponds to the light being scattered entirely in a forward direction ($\theta = 0°$) while

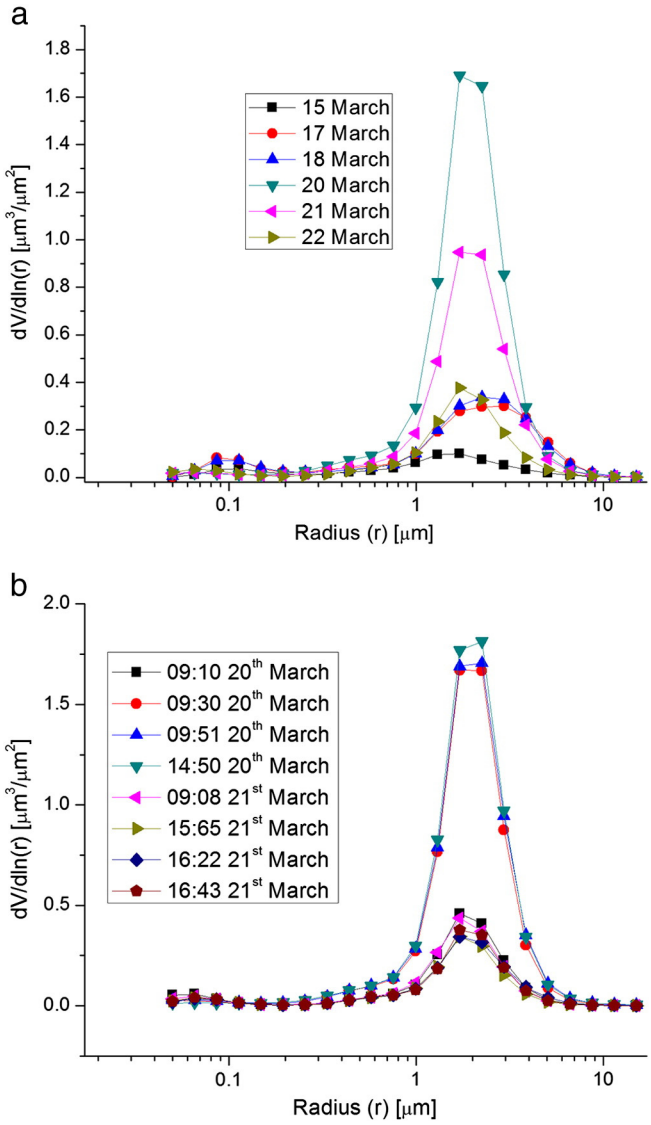

Fig. 6. (a) AERONET volume size distributions over Lahore during dusty and non-dusty days. (b) Diurnal variations in AERONET volume size distribution on the 20th and 21st of March.

ASY = −1 corresponds to the light being scattered entirely in a backward direction (θ = 180°). Where ASY = 0 this corresponds to the light being scattered uniformly in all directions (isotropic scattering). The variations in the total ASY (ASY-T) for both modes (fine and coarse), and the coarse ASY (ASY-C) for dusty and non-dusty days over Lahore are shown in Fig. 7 (c & d). The ASY showed marked spectral variation over the study period, with higher values at shorter wavelengths. ASY-C values on non-dusty days varied from 0.80 at 440 nm to 0.73 at 1020 nm, and on dusty days from 0.78 at 440 nm to 0.73 at 1020 nm. Similarly, ASY-T values varied from 0.71 at 440 nm to 0.69 at 1020 nm on non-dusty days, and from 0.75 at 440 nm to 0.72 at 1020 nm on dusty days. The ASY-T values were higher in the near infrared region than in the visible spectral region on non-dusty days, with the reverse being true on dusty days. ASY-C values were higher in the visible spectral region than in the near infrared region on both non-dusty and dusty days. The higher values (over 0.80 at 440 nm) reflect a dominance of dust aerosols over absorbing anthropogenic aerosols. Fig. 7e reveals the diurnal variations in ASY-T during dusty days (March 20th and 21st). The results suggested that these ASY variations on the 20th of March are high as compared to the 21st of March. The differences in diurnal variations in ASY on dusty days at a wavelength of 440 nm are in the range of 0.008–0.04. Likewise, the differences in diurnal variations in ASY at 1020 nm on dusty days are in the range of 0.003–0.02. The diurnal variations of AOD, aerosol VSD, SSA, and ASY are important for accurate calculations of the radiative effect of dust aerosols on the surface. Christopher, Wang, Ji, and Tsay (2003) reported that the change of 0.1 AOD can lead up to 10 W m^{-2} downward shortwave irradiance changes at the surface. In the present study the change in diurnal variations of AOD varies in the range of 0.07–0.21. The resulting changes in the radiative forcing ranges from 5 W m^{-2} to 20 W m^{-2} at the surface and from 3 W m^{-2} to 10 W m^{-2} at the TOA. Christopher and Wang (2004) analyzed that a 10% variation of AOD will generally result in 5–8% change of TOA forcing, and in 8–12% change of forcing at the surface. Therefore, the diurnal variations of aerosol properties in dust regions should be carefully considered for more precise estimation of forcing calculation (Christopher & Wang, 2004; Wang, Xia, Wang, & Christopher, 2004).

The remote sensing satellite sensors, such as the Total Ozone Mapping Spectrometer, the Multi-angle Imaging Spectroradiometer, and the MODIS, are useful for retrieving aerosol properties from space. Since MODIS passes a specific area only once per day in the tropical regions, it can capture only one phase of any AOD diurnal cycle (Wang et al., 2003). Therefore, this low temporal resolution makes it difficult to capture the diurnal aerosol variations.

3.5. Refractive index (RI)

The real n (λ) and imaginary k (λ) components of the refractive index (RI) provide information on whether aerosols belong to scattering or absorbing types. High n (λ) values indicate scattering types of aerosols and high k (λ) values absorbing types (Alam et al., 2012; Bohren & Huffman, 1983; Sinyuk, Torres, & Dubovik, 2003). The RI values for mineral dust particles have been reported to be 1.53 ± 0.05 for n (λ) and ~0.006 or less for k (λ) (Koepke, Hess, Schult, & Shettle, 1997; Levin, Joseph, & Mekler, 1980; Shettle & Fenn, 1979; Sokolik, Andronova, & Johnson, 1993; WMO, 1983). Cheng, Liu, Lu, Xu, and Li (2006), Cheng, Wang, Xu, Li, and Tian (2006) and Alam et al. (2012) reported that the n (λ) values were larger at a higher wavelength (1020 nm) than at a shorter wavelength (440 nm) due to greater absorption by coarse particles in the near infrared band. The n (λ) and k (λ) values at wavelengths 440, 675, 870 and 1020 nm over Lahore are shown in Fig. 8a. The n (λ) values on a dusty day (20th of March, 2012) for wavelengths 440, 675, 870 and 1020 nm, as retrieved by AERONET over Lahore, were ~1.56, 1.52, 1.50, and 1.49, respectively. We found that the n (λ) values on dusty days were higher for shorter wavelengths, reflecting the predominance of mineral dust particles, which are scattering rather than absorbing. This is due to the n (λ) values for dust aerosols being greater than those for anthropogenic aerosols (Liu, Zheng, Li, & Wu, 2008). Our results are in close agreement with those reported by Alam et al. (2012) over Lahore during the summer season of 2010. Similar results for n (λ) have also been reported over Kanpur, in India, during the summer (Prasad & Singh, 2007; Prasad et al., 2007; Tripathi et al., 2005). The k (λ) values provide information of the absorption capacity of the medium (Sokolik & Toon, 1999). Over our study region the k (λ) values on dusty days for wavelengths 440, 675, 870 and 1020 nm were 0.00275, 0.00087, 0.00067, and 0.00064 (20th of March, 2012) and 0.00295, 0.00094, 0.00075, and 0.00072 (21st of March), respectively. The AERONET k (λ) values were found to be lower for dusty days than for non-dusty days. For non-dusty days, the k (λ) values fluctuated between 0.0099 (440 nm) and 0.0037 (1020 nm), while for dusty days the k (λ) values fluctuated between 0.0027 (440 nm) and 0.00046 (1020 nm). This shows that the k (λ) values for the dominant mineral dust aerosols were lowest on dusty days (see Fig. 8b), indicating their non-absorbing nature. The SSA thus tends to increase during dust storms due to this reduction in absorption. An increase in SSA was also found to be common

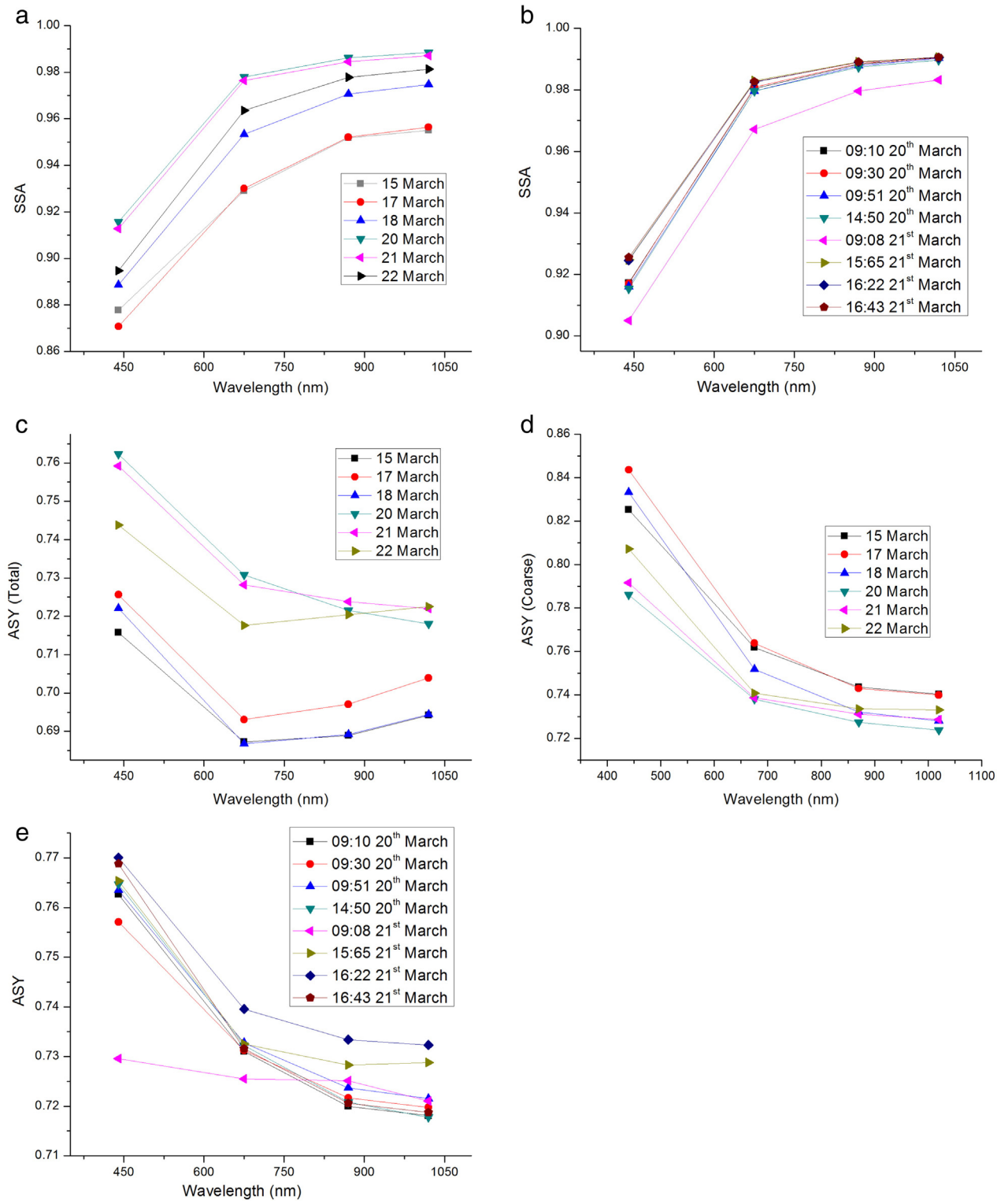

Fig. 7. Spectral variations in AERONET retrieved (a) SSA, (c) ASY-T, and (d) AST-C over Lahore, during dusty and non-dusty days. Diurnal variations in AERONET (b) SSA, (e) ASY-T on the 20th and 21st of March.

during dust storms by Kubilay, Cokacar, and Oguz (2003). The k (λ) values from our results were found to be higher on non-dusty days than on dusty days, revealing the presence of more absorbing anthropogenic aerosols (Alam, Blaschke, et al., 2011). Overall variations in RI (both real and imaginary components) within our study reveal that mineral dust aerosols are more dominant on dusty days than on non-dusty days.

3.6. Aerosol radiative forcing (ARF)

ARF is defined as the difference in the net (down minus up) solar flux (solar plus long wave; in W m^{-2}), with and without aerosols, i.e.

$$\Delta F = \left(F_{a\downarrow} - F_{a\uparrow}\right) - \left(F_{0\downarrow} - F_{0\uparrow}\right)$$

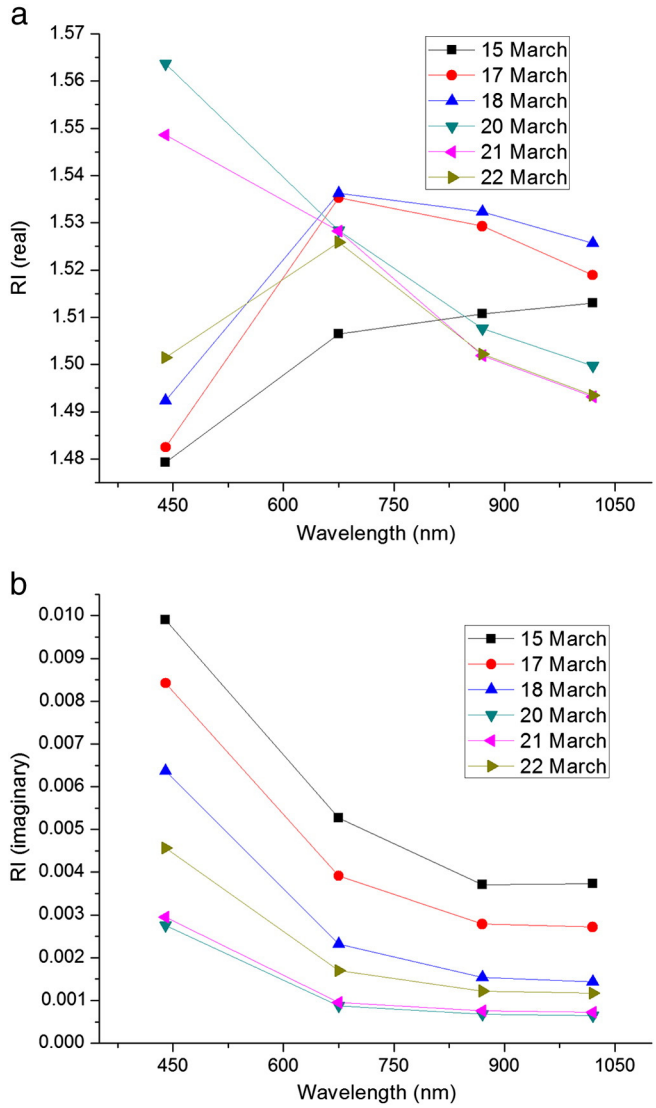

Fig. 8. Spectral variations in AERONET retrieved (a) real components of RI (b) imaginary components of RI, during dusty and non-dusty days.

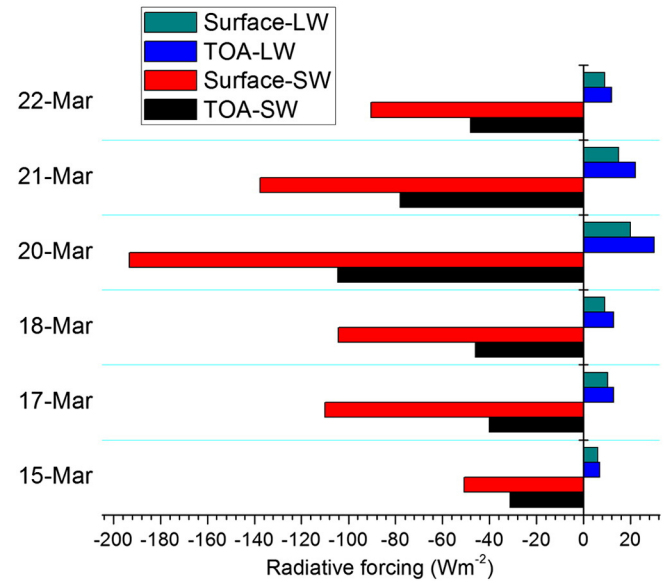

Fig. 9. Shortwave and longwave aerosol radiative forcing at the TOA and at the earth's surface, during dusty and non-dusty days.

where ΔF denotes the irradiance (downwelling or upwelling, W m^{-2}) and ($F_{\downarrow} - F_{\uparrow}$) denotes the net irradiance (down minus up), computed with aerosol (F_a), and without aerosol (F_0), either at the TOA or at the earth's surface.

We calculated the net flux at the TOA and at the earth's surface for both short wavelengths (0.3–4.0 μm) and long wavelengths (4.0–100 μm) using the SBDART model. The SBDART model was developed by the atmospheric science community and has been widely used to calculate radiative transfers. The input parameters for ARF calculations were the AOD, SSA, ASY and surface albedo. The optical parameters (AOD, SSA, and ASY) were taken from the Lahore AERONET site, and the surface albedo values were obtained from MODIS data. There are also some other input parameters in the model such as the solar zenith angle, which is calculated using a small code in the SBDART model by specifying a particular date, time, latitude and longitude.

The daily average SW and LW ARF variations at the TOA and at the earth's surface during the study period are shown in Fig. 9. Both SW and LW ARF values reached a maximum on dusty days. The SW ARF values (on both dusty and non-dusty days) ranged between −50 W m^{-2} and −194 W m^{-2} at the earth's surface, and between −31 W m^{-2} and −105 W m^{-2} at the TOA. The LSW ARF values (on both dusty and non-dusty days) ranged between +6 W m^{-2} and +20 W m^{-2} at the earth's surface, and between +7 W m^{-2} and +30 W m^{-2} at the TOA. The average SW and LW ARF values at the earth's surface on both dusty and non-dusty days were −114 ± 40 W m^{-2} and +12 ± 4 W m^{-2}, respectively, while the average SW and LW ARF values at the TOA on both dusty and non-dusty days were −58 ± 25 W m^{-2} and +16 ± 7 W m^{-2}, respectively. LW radiations are therefore shown to produce significant warming on dusty days, both at the earth's surface and at the TOA. Alam et al. (2012) found the ARF at the TOA to be between −16 and −31 W m^{-2} over Lahore and between −14 and −21 W m^{-2} over Karachi, while at the earth's surface it was found to be between −70 and −112 W m^{-2} for Lahore and between −52 and −73 W m^{-2} for Karachi. The global mean clear-sky ARF values at the TOA and at the earth's surface have been found by previous authors to be negative (Ge et al., 2010; Kim & Ramanathan, 2008; Yu, Cheng, Chen, & Liu, 2006). Thomas, Chalmers, Harris, Grainger, and Highwood (2013) reported that global and annual mean aerosol radiative effects were found to be −6.7 ± 3.9 W m^{-2} and −12 ± 6 W m^{-2} at the TOA and at the surface, respectively. The ARF values at the earth's surface in north-western China were found to be between −7.9 and −35.8 W m^{-2} (Ge et al., 2010), which are higher than surface ARF values for Lahore. Our surface ARF values over Lahore for March 2012 are comparable with surface ARF values reported from Yulin, China (Huizheng et al., 2009), which were between −38 and −108 W m^{-2}, but our own TOA ARF values are higher. Kim, Sohn, Nakajima, and Takamura (2005) calculated ARF values of between −13 and −43 W m^{-2} for three ground sites in eastern Asia, which is lower than the range obtained from our own results. The ARF values reported from India by Alam, Qureshi, and Blaschke (2011) were between −19 and −87 W m^{-2} at the earth's surface and between +2 and −26 W m^{-2} at the TOA during the entire dust period from April to May in 2005. The surface ARF values reported by Pandithurai et al. (2008) from New Delhi in 2006 were between −39 W m^{-2} (in March) and −99 W m^{-2} (in June); these values are slightly lower but still comparable to our own results reported herein. ARF values of between −45 and −65 W m^{-2} at the earth's surface have been reported from Morocco (Bierwirth et al., 2009), Chinnam, Dey, Tripathi, and Sharma (2006) reported ARF values at the TOA over Kanpur, India during a dust storm of between −12 and +7 W m^{-2}, and ARF values calculated by Li, Vogelmann, and Ramanathan (2004) and Yoon, Won, Omar, Kim, and Sohn (2005) over the Middle East and the Sahara Desert are also lower than our own values. Our ARF values are thus higher than all

previous values reported from dust storm events, both at the earth's surface and at the TOA. There is a large difference between the ARF values at the TOA and those at the earth's surface indicating that solar radiation is being absorbed within the atmosphere, which results in the atmosphere becoming warmer but the earth's surface becoming cooler (Alam, Blaschke, et al., 2011; Alam, Sahar, & Yaseen, 2013; Alam et al., 2012; Ge et al., 2010; Miller and Tegen, 1999). The difference in ARF values can affect the stability and dynamic system of the atmosphere (Li et al., 2010).

4. Conclusion

Aerosol characteristics, including their optical and radiative properties, have been analyzed during super dust storms over the Middle East and southwest Asia, using MODIS and AERONET measurements. The MODIS AOD values were found to be higher than 4 (or even 5 in some cases) in the Gulf Regions, Saudi Arabia, Oman, over the Arabian Sea, and in Iran. Dust derived from the Gulf Regions, southeast Iran, and southwest Pakistan traveled towards major cities in Pakistan, resulting in high AOD values (>2) being recorded in Multan, Faisalabad, and Lahore. The aerosol optical properties (VSD, SSA, ASY, and RI) revealed that dust aerosols dominated anthropogenic aerosols over the Lahore mega city. The radiative transfer model simulation revealed that dust aerosol SW ARF produces cooling effects at both the TOA and the earth's surface. In contrast, dust aerosol LW ARF produces warming effects at both the TOA and the earth's surface.

References

Alam, K., Blaschke, T., Madl, P., Mukhtar, A., Hussain, M., Trautmann, T., et al. (2011). Aerosol size distribution and mass concentration measurements in various cities of Pakistan. *Journal of Environmental Monitoring*, *13*, 1944–1952.

Alam, K., Qureshi, S., & Blaschke, T. (2011). Monitoring spatio-temporal aerosol patterns over Pakistan based on MODIS, TOMS and MISR satellite data and a HYSPLIT model. *Atmospheric Environment*, *45*, 4641–4651.

Alam, K., Sahar, N., & Yaseen, I. (2013). Aerosol characteristics and radiative forcing during pre-monsoon and post-monsoon seasons in an urban environment. *Aerosol and Air Quality Research*. http://dx.doi.org/10.4209/aaqr.2013.05.0154.

Alam, K., Trautmann, T., & Blaschke, T. (2011). Aerosol optical properties and radiative forcing over mega city Karachi. *Atmospheric Research*, *101*, 773–782.

Alam, K., Trautmann, T., & Blaschke, T. (2012). Aerosol optical and radiative properties during summer and winter seasons over Lahore and Karachi. *Atmospheric Environment*, *50*, 234–245.

Almeida, G. A. (1987). On the variability of desert aerosol radiative characteristics. *Journal of Geophysical Research*, *92*, 3017–3026.

Alpert, P., Kaufman, Y. J., Shay-El, Y., Tanre, D., da Silva, A., Schubert, S., et al. (1998). Quantification of dust-forced heating of the lower troposphere. *Nature*, *395*, 367–370.

Alpert, P., Kishcha, P., Shtivelman, A., Krichak, S. O., & Joseph, J. H. (2004). Vertical distribution of Saharan dust based on 2.5-year model predictions. *Atmospheric Research*, *70*, 109–130.

Bierwirth, E., Wendisch, M., Ehrlich, A., Heese, B., Tesche, M., Althausen, D., et al. (2009). Spectral surface albedo over Morocco and its impact on the radiative forcing of Saharan dust. *Tellus*, *61B*, 252–269.

Bohren, C. F., & Huffman, D. R. (1983). *Absorption and scattering of light by small particles*. John Wiley (550 pp.).

Chameides, W. L., Yu, H., Liu, S. C., Bergin, M., Zhou, X., Mearns, L., et al. (1999). Case study of the effects of atmospheric aerosols and regional haze on agriculture: An opportunity to enhance crop yields in China through emission controls. *Proceeding of the National Academy of Sciences*, *96*, 13,626–13,633.

Charlson, R. J., & Heintzenberg, J. (1995). *Aerosol forcing of climate*. Chichester, UK: John Wiley and Sons.

Cheng, T., Liu, Y., Lu, D., Xu, Y., & Li, H. (2006). Aerosol properties and radiative forcing in Hunshan Dake desert, northern China. *Atmospheric Environment*, *40*, 2169–2179.

Cheng, T., Wang, H., Xu, Y., Li, H., & Tian, L. (2006). Climatology of aerosol optical properties in northern China. *Atmospheric Environment*, *40*, 1495–1509.

Chinnam, N., Dey, S., Tripathi, S. N., & Sharma, M. (2006). Dust events in Kanpur, northern India: Chemical evidence for source and implications to radiative forcing. *Geophysical Research Letters*, *33*. http://dx.doi.org/10.1029/2005GL025278.

Christopher, S. A., & Wang, J. (2004). Intercomparison between MISR and Sunphotometer AOT in dust source regions over china: Implication for satellite retrievals and radiative forcing calculations. *Tellus*, *56B*, 451–456.

Christopher, S. A., Wang, J., Ji, Q., & Tsay, S. -C. (2003). Estimation of shortwave dust aerosol radiative forcing during PRIDE. *Journal of Geophysical Research*, *108*, 8596. http://dx.doi.org/10.1029/2002JD002787.

Chu, D., Kaufman, Y., Ichoku, C., Remer, L., Tanr'e, D., & Holben, B. (2002). Validation of MODIS aerosol optical depth retrieval over land. *Geophysical Research Letters*, *29*, 8007. http://dx.doi.org/10.1175/JAS3385.1.

Dey, S., Tripathi, S. N., Singh, R. P., & Holben, B. N. (2004). Influence of dust storms on the aerosol optical properties over the Indo-Gangetic basin. *Journal of Geophysical Research*, *109*, D20211. http://dx.doi.org/10.1029/2004JD004924.

Draxler, R. R., & Rolph, G. D. (2003). HYSPLIT (HYbrid Single-Particle Lagrangian Integrated Trajectory) Model access via the NOAA ARL READY Website, NOAA Air Resour. Lab., Silver Spring, Md. Available at http://www.arl.noaa.gov/ready/hysplit4.html

Dubovik, O., Smirnov, A., Holben, B. N., King, M.D., Kaufman, Y. J., Eck, T. F., et al. (2000). Accuracy assessments of aerosol optical properties retrieved from Aerosol Robotic Network (AERONET) Sun and sky radiance measurements. *Journal of Geophysical Physical Research*, *105*, 9791–9806.

Dubovik, O., Smirnov, A., Holben, B. N., King, M.D., Kaufman, Y. J., Eck, T. F., et al. (2002). Variability of absorption and optical properties of key aerosol types observed in worldwide locations. *Journal of Atmospheric Science*, *59*, 590–608.

Forster, P., Ramaswamy, V., Artaxo, P., Berntsen, T., Betts, R., Fahey, W. D., et al. (2007). Changes in atmospheric constituents and in radiative forcing. *Climate Change 2007: The Physical Science Basis, Working Group I to the Fourth Assessment Report of the Intergovernmental Panel on Climate Change* (pp. 129–234). United Kingdom and New York: Cambridge University Press.

Ge, J. M., Su, J., Ackerman, T. P., Fu, Q., Huang, J. P., & Shi, J. S. (2010). Dust aerosol optical properties retrieval and radiative forcing over northwestern China during the 2008 China–U.S. joint field experiment. *Journal of Geophysical Research*, *115*(D00k12). http://dx.doi.org/10.1029/2009JD013263.

Golitsyn, G., & Gillette, D. A. (1993). Introduction: A joint Soviet — American experiment for the study of Asian desert dust and its impact on local meteorological conditions and climate. *Atmospheric Environment, Part A*, *27A*(16), 2467–2470.

Hansen, J., Sato, M., & Ruedy, R. (1997). Radiative forcing and climate response. *Journal of Geophysical Research*, *102*(D6), 6831–6864.

Holben, B. N., Eck, T. F., Slutsker, I., Tanré, D., Buis, J. P., Setzer, A., et al. (1998). AERONET-A federated instrument network and data archive for aerosol characterization. *Remote Sensing of Environment*, *66*, 1–16.

Houghton, J., Ding, Y., Griggs, D. J., Noguer, M., Linden, P. J., & Xiaosu, E. (2001). *Climate Change 2001: The Scientific Basis: Contributions of Working Group I to the Third Assessment Report of the Intergovernmental Panel on Climate Change*. New York: Cambridge Univ Press.

Huang, J., Fu, Q., Su, J., Tang, Q., Minnis, P., Hu, Y., et al. (2009). Taklimakan dust aerosol radiative heating derived from CALIPSO observations using the Fu -Liou radiation model with CERES constraints. *Atmosphere Chemistry Physics*, *9*, 4011–4021.

Huizheng, C., Xiaoye, Z., Alfraro, S., Chatenet, B., Gomes, L., & Jianqi, Z. (2009). Aerosol optical properties and its radiative forcing over Yulin, China in 2001 and 2002. *Advances in Atmospheric Sciences*, *26*, 564–576.

Hunt, W. H., Winker, D.M., Vaughan, M.A., Powell, K. A., Lucker, P. L., & Weimer, C. (2009). CALIPSO lidar description and performance assessment. *Journal of Atmospheric and Oceanic Technology*, *26*, 1214–1228.

Husar, R. B., Tratt, D.M., Schichtel, B.A., Falke, S. R., Li, F., Jaffe, D., et al. (2001). Asian dust event of April 1998. *Journal of Geophysical Research*, *06*, 18317–18330.

Kaufman, Y., Tanre', D., & Boucher, O. (2002). A satellite view of aerosols in the climate system. *Nature*, *419*, 215–223.

Kazmi, A., & Vaidya, S. K. (2012). *March 20 [local time zone]) bad weather hits Fujairah air traffic*. Gulf News (Accessed March 19, 2012).

Kim, D. H., & Ramanathan, V. (2008). Solar radiation budget and radiative forcing due to aerosols and clouds. *Journal of Geophysical Research*, *113*(D02203). http://dx.doi.org/10.1029/2007JD008434.

Kim, D. O. H., Sohn, B. J., Nakajima, T., & Takamura, T. (2005). Aerosol radiative forcing over East Asia determined from ground-based solar radiation measurements. *Journal of Geophysical Research*, *110*(D10S22). http://dx.doi.org/10.1029/2004JD004678.

Kim, D. H., Sohn, B. J., Nakajima, T., Takamura, T., Takemura, T., Choi, B. C., et al. 2004a. Aerosol optical properties over East Asia determined from ground-based sky radiation measurements. *Journal of Geophysical Research*, *109*, D02209. http://dx.doi.org/10.1029/2003JD003387.

Kim, S. W., Yoon, S.C., Jefferson, A., Won, J. G., Dutton, E. G., Ogren, J. A., et al. 2004b. Observation of enhanced water vapor in Asian dust layer and its effect on atmospheric radiative heating rates. *Geophysical Research Letters*, *31*, L18113. http://dx.doi.org/10.1029/2004GL020024.

Koepke, P., Hess, M., Schult, I., & Shettle, E. P. (1997). *Global aerosol data set Rep., 243*. Hamburg, Germany: Max Planck Inst. for Meteorol, 44.

Kubilay, N., Cokacar, T., & Oguz, T. (2003). Optical properties of mineral dust outbreaks over the northeastern Mediterranean. *Journal of Geophysical Research*, *108*(D21), 4666.

Kutiel, H., & Furman, H. (2003). Dust storms in the Middle East: Sources of origin and their temporal characteristics. *Indoor Built Environment*, *12*, 419–426.

Levin, Z., Joseph, J. H., & Mekler, Y. (1980). Properties of Sharav (Khamsin) dust — Comparison of optical and direct sampling data. *Journal of Atmospheric Science*, *37*, 182–191.

Levy, R. C., Remer, L. A., Mattoo, S., Vermote, E. F., & Kaufman, Y. J. (2007). Second-generation operational algorithm: Retrieval of aerosol properties over land from inversion of Moderate Resolution Imaging Spectroradiometer spectral reflectance. *Journal of Geophysical Research*, *112*, D13211. http://dx.doi.org/10.1029/2006JD007811.

Li, F., Vogelmann, A.M., & Ramanathan, V. (2004). Saharan dust aerosol radiative forcing measured from space. *Journal of Climate*, *17*(13), 2558–2571.

Li, Z., Lee, K. -H. O., Wang, Y., Xin, J., & Hao, W. -M. (2010). First observation-based estimates of cloud-free aerosol radiative forcing across China. *Journal of Geophysical Research*, *115*, D00K18. http://dx.doi.org/10.1029/2009JD013306.

Liao, H., & Seinfeld, J. H. (1998). Radiative forcing by mineral dust aerosols: Sensitivity to key variables. *Journal of Geophysical Research*, *103*(D24), 31,637–31,645.

Liu, J., Zheng, Y., Li, Z., & Wu, R. (2008). Ground-based remote sensing of aerosol optical properties in one city in Northwest China. *Atmospheric Research*, *89*, 194–205.

Middleton, N. J. (1986). Geography of dust storms in southwest Asia. *Journal of Climate*, *6*, 183–196.

Miller, R. L., Perlwitz, J., & Tegen, I. (2004). Feedback by dust radiative forcing upon dust emission through the planetary boundary layer. *Journal of Geophysical Research*, *109*, D24209. http://dx.doi.org/10.1029/2004JD004912.

Miller, R. L., & Tegen, I. (1998). Climate response to soil dust aerosols. *Journal of Climate*, *11*, 3247–3267.

Miller, R. L., & Tegen, I. (1999). Radiative forcing of a tropical direct circulation by soil dust aerosols. *Journal of Atmospheric Science*, *56*, 2403–2433.

Miller, R. L., Tegen, I., & Perlwitz, J. (2004). Surface radiative forcing by soil dust aerosols and the hydrologic cycle. *Journal of Geophysical Research*, *109*, D04203. http://dx.doi.org/10.1029/2003JD004085.

Mishra, S. K., & Tripathi, S. N. (2008). Modeling optical properties of mineral dust over the Indian Desert. *Journal of Geophysical Research*, *113*, D23201. http://dx.doi.org/10.1029/2008JD010048.

NASA Earth Observatory Natural Hazards (2012). Dust storm over Pakistan. http://earthobservatory.nasa.gov/NaturalHazards/view.php?id=77450

Nastos, P. T., Kampanis, N. A., Giaouzaki, K. N., & Matzarakis, A. (2011). Environmental impacts on human health during a Saharan dust episode at Crete Island, Greece. *Meteorologische Zeitschrift*, *20*(5), 517–529.

Pandithurai, G., Dipu, S., Dani, K. K., Tiwari, S., Bisht, D. S., Devara, P. C. S., et al. (2008). Aerosol radiative forcing during dust events over New Delhi, India. *Journal of Geophysical Research*, *113*(D13209). http://dx.doi.org/10.1029/2008JD009804.

Parungo, F., King, Y., & Zhu, C. (1995). *Asian dust storms and their effects on radiation and climate. STC Technical Report 2959, Part1*Hampton, VA: Science and Technology Corporation.

Prasad, A. K., & Singh, R. P. (2007). Changes in aerosol parameters during major dust storm events (2001–2005) over the Indo-Gangetic Plains using AERONET and MODIS data. *Journal of Geophysical Research*, *112*(D09208). http://dx.doi.org/10.1029/2006JD007778.

Prasad, A. K., Singh, S., Chauhan, S. S., Srivastava, M. K., Singh, R. P., & Singh, R. (2007). Aerosol radiative forcing over the Indo-Gangetic Plains during major dust storms. *Atmospheric Environment*, *41*, 6289–6301.

Prospero, J. M., & Carlson, T. N. (1972). Vertical and areal distribution of Saharan dust over the western Equatorial North Atlantic Ocean. *Journal of Geophysical Research*, *77*(27), 5255–5265.

Prospero, J. M., Ginoux, P., Torres, O., Nicholson, S. E., & Gill, T. E. (2002). Environmental characterization global sources of atmospheric soil dust identified with the Nimbus 7 total ozone mapping spectrometer (TOMS) absorbing aerosol product. *Reviews of Geophysics*, *40*(1), 1002.

Ramanathan, V., Crutzen, P. J., Kiehl, J. T., & Rosenfeld, D. (2001). Aerosols, climate, and the hydrologic cycle. *Science*, *294*, 2119–2124.

Remer, L. A., Kaufman, Y. J., Tanr´e,, D., Mattoo, S., Chu, D. A., Martins, J. V., et al. (2005). The MODIS aerosol algorithm, products and validation. *Journal of Atmospheric Science*, *62*, 947–973.

Ricchiazzi, P., Yang, S., Gautier, C., & Sowle, D. (1998). SBDART: A research and teaching software tool for plane-parallel radiative transfer in the earth's atmosphere. *Bulletin of American Meteorological Society*, *79*, 2101–2114.

Sharma, D., Singh, D., & Kaskaoutis, D.G. (2012). Impact of two intense dust storm on aerosol characteristics and radiative forcing over Patiala, Northwestern India. *Advances in Meteorology*. http://dx.doi.org/10.1155/2012/956814 (Article ID 956814).

Shettle, E. P., & Fenn, R. W. (1979). Models of aerosols lower troposphere and the effect of humidity variations on their optical properties. *AFCRL Tech. Rep. 79 0214*. Air Force Cambridge Res. Lab., Hanscom Air Force Base, Mass (100 pp.).

Singh, R. P., Prasad, A. K., Kayetha, V. K., & Kafatos, M. (2008). Enhancement of oceanic parameters associated with dust storms using satellite data. *Journal of Geophysical Research*, *113* (Article ID C11008).

Sinha, A., & Harries, J. E. (1997). Possible change in climate parameters with zero net radiative forcing. *Geophysical Research Letters*, *24*(19), 2355–2358.

Sinyuk, A., Torres, O., & Dubovik, O. (2003). Combined use of satellite and surface observations to infer the imaginary part of the refractive index of Saharan dust. *Geophysical Research Letters*, *30*(2), 1081. http://dx.doi.org/10.1029/2002GL016189.

Smirnov, A., Holben, B. N., Eck, T. F., Dubovik, O., & Slutsker, I. (2000). Cloud screening and quality control algorithms for the AERONET data base. *Remote Sensing of Environment*, *73*, 337–349.

Sokolik, I., Andronova, A., & Johnson, T. C. (1993). Complex refractive index of atmospheric dust aerosols. *Atmospheric Environment, Part A: General Topics*, *27A*(16), 2495–2502.

Sokolik, I. N., & Toon, O. B. (1999). Incorporation of mineralogical composition into models of the radiative properties of mineral aerosol from UV to IR wavelengths. *Journal of Geophysical Research*, *104*, 9423–9444.

Sokolin, I. N., & Toon, O. B. (1996). Direct forcing by air borne mineral aerosol. *Nature*, *381*, 681–683.

Tegen, I., & Fung, I. (1994). Modeling of mineral dust in the atmosphere: Sources, transport, and optical thickness. *Journal of Geophysical Research*, *99*(D11). http://dx.doi.org/10.1029/94JD01928.

Tegen, I., Lacis, A. A., & Fung, I. (1996). The influence on climate forcing of mineral aerosols from disturbed soils. *Nature*, *380*(6573), 419–422.

Tegen, I., Hollrig, P., Chin, M., Fung, I., Jacob, D., & Penner, J. (1997). Contribution of different aerosol species to the global aerosol extinction optical thickness: Estimates from model results. *Journal of Geophysical Research*, *102*, 23,895–23,915.

Thomas, G. E., Chalmers, N., Harris, B., Grainger, R. G., & Highwood, E. J. (2013). Regional and monthly and clear-sky aerosol direct radiative effect (and forcing) derived from the GlobAEROSOL-AATSR satellite aerosol product. *Atmospheric Chemistry and Physics*, *13*, 393–410.

Tripathi, S. N., Dey, S., Chandel, A., Srivastava, S., Singh, R. P., & Holben, B. N. (2005). Comparison of MODIS and AERONET derived aerosol optical depth over the Ganga Basin, India. *Annales Geophysicae*, *23*, 1093–1101.

Wang, J., Christopher, S. A., Reid, J. S., Maring, H., Savoie, D., Holben, B. N., et al. (2003). GOES 8 retrieval of dust aerosol optical thickness over Atlantic Ocean during PRIDE. *Journal of Geophysical Research*, *108*(D19), 8595. http://dx.doi.org/10.1029/2002JD002494.

Wang, J., Xia, X., Wang, P., & Christopher, S. A. (2004). Diurnal variability of dust aerosol optical thickness and angstrom exponent over dust source regions in China. *Geophysical Research Letters*, *31*, L08107. http://dx.doi.org/10.1029/2003GL019580.

Winker, D.M., Hunt, W. H., & McGill, M. J. (2007). Initial performance assessment of CALIOP. *Geophysical Research Letters*, *34*, L19803. http://dx.doi.org/10.1029/2007GL030135.

Winker, D.M., Pelon, J., & McCormick, M. P. (2003). The CALIPSO mission: Spaceborne lidar for observation of aerosols and clouds. *Proceedings of SPIE*, *4893*, 1–11.

World Meteorological Organization (WMO) (1983). *Radiation commission of IAMAP meeting of experts on aerosols and their climatic effects, Rep. WCP55, Geneva, Switzerland.*

Xia, X., Wang, P., Chen, H., Gouloub, P., & Zhang, W. (2005). Ground-based remote sensing of aerosol optical properties over north China in spring. *Journal of Remote Sensing*, *9*, 429–437.

Xia, X., & Zong, X. (2009). Shortwave versus Longwave Direct Radiative Forcing by Taklimakan Dust Aerosols. *Geophysical Research Letter*, *36*, L07803. http://dx.doi.org/10.1029/2009GL037237.

Yoon, S.C., Won, J. G., Omar, A. H., Kim, S. W., & Sohn, B. J. (2005). Estimation of the radiative forcing by key aerosol types in worldwide locations using a column model and AERONET data. *Atmospheric Environment*, *39*(35), 6620–6630.

Yu, X., Cheng, T., Chen, J., & Liu, Y. (2006). A comparison of dust properties between China continent and Korea, Japan in East Asia. *Atmospheric Environment*, *40*, 5787–5797.

Zheng, Y., Liu, J., Wu, R., Li, Z., Wang, B., & Tamio, T. (2008). Seasonal statistical characteristics of aerosol optical properties at a site near dust region in China. *Journal of Geophysical Research*, *113*, D16205. http://dx.doi.org/10.1029/2007JD009384.

Zhu, A., Ramanathan, A., Li, F., & Kim, D. (2007). Dust plumes over the Pacific Indian, and Atlantic oceans: Climatology and radiative impact. *Journal of Geophysical Research*, *112*, D16208. http://dx.doi.org/10.1029/2007JD008427.